Tuning Electronic and Magnetic Properties of Wurtzite ZnO Nanosheets by Surface Hydrogenation

5 AUTHORS, INCLUDING:

Yafei Li
Nanjing Normal University
48 PUBLICATIONS **2,052** CITATIONS

SEE PROFILE

Zhen Zhou
Nankai University
213 PUBLICATIONS **6,996** CITATIONS

SEE PROFILE

Yongsheng Chen
Georgia Institute of Technology
315 PUBLICATIONS **17,789** CITATIONS

SEE PROFILE

Zhongfang Chen
University of Puerto Rico at Rio Piedras
221 PUBLICATIONS **8,056** CITATIONS

SEE PROFILE

Tuning Electronic and Magnetic Properties of Wurtzite ZnO Nanosheets by Surface Hydrogenation

Qing Tang,[†] Yafei Li,[†] Zhen Zhou,[*,†] Yongsheng Chen,[‡] and Zhongfang Chen[§]

Institute of New Energy Material Chemistry, Key Laboratory of Advanced Energy Materials Chemistry, Ministry of Education, Nankai University, Tianjin 300071, P. R. China, School of Civil and Environmental Engineering, Georgia Institute of Technology, Atlanta, Georgia 30332, and Department of Chemistry, Institute for Functional Nanomaterials, University of Puerto Rico, Rio Piedras Campus, San Juan, PR 00931

ABSTRACT Through density functional theory computations, we systematically investigated the structural, electronic, and magnetic properties as well as the relative stabilities of fully and partially hydrogenated ZnO nanosheets. Unlike bare ZnO nanosheets terminating with polar {0001} surfaces, their hydrogenated counterparts preserve the initial wurtzite configuration. Full hydrogenation is more favorable energetically for thinner ZnO nanosheets, whereas semihydrogenation at O sites is preferred for thicker ones. Moreover, semiconductor → half-metal → metal transition occurs with nonmagnetic → magnetic transfer upon adopting surface hydrogenation and increasing sheet thickness. The predicted diverse and tunable electronic and magnetic properties endow ZnO nanosheets potential applications in electronics and spintronics.

KEYWORDS: ZnO • nanosheets • electronic structure • magnetism

INTRODUCTION

Zinc oxide (ZnO) clearly distinguishes itself from other II−VI semiconductors. The rather unique characteristics, such as wide energy gap (∼3.4 eV), large exciton binding energy (60 meV), and extraordinary piezoelectric and optical properties (1), endow ZnO a wide range of technological applications in UV-light emitting diodes (2), solar cells (3), photocatalysts (4), etc. At the nanoscale, ZnO brings us more sweet surprises (5−7). The versatile chemical bonding of ZnO leads to probably the richest family of nanostructures among all materials (8); nanowires (9), nanotubes (10), nanobelts (11), nanorods (12), nanobridges/nanonails (13), nanofilms (14), and nanorings (15) have been successfully synthesized through a variety of experimental techniques. These low-dimensional structures have demonstrated extraordinary electrical and optical performances compared with the bulk crystalline ZnO, and are promising candidates for many novel applications in transparent electronics, gas sensors, transducers, solar cells, and biomedical devices.

At ambient conditions, bulk ZnO adopts the wurtzite structure as its thermodynamically stable phase. Amazingly, at the nanoscale, ZnO can also form two-dimensional (2D) nanosheets besides other various nanostructures. Theoretically, Topsakal et al. (16) predicted that ZnO, in analogy to graphene and boron nitride (BN) monolayers, can form a hexagonal honeycomb structure in which Zn and O atoms are arranged in planar 3-fold coordination instead of the bulk-like tetrahedral configuration. Kulkarni et al. (17) predicted a phase transformation from wurtzite to a graphite-like hexagonal structure in ZnO nanowires under tensile loading. Furthermore, the fascinating ferromagnetism and unusual electronic properties associated with one-dimensional (1D) ZnO nanoribbons (18−21) derived from either monolayer or multilayer sheets heavily depend on the ribbons' width, thickness and edge modification. Experimentally, great progress has been made in synthesizing ZnO nanosheets (22−27). Tusche et al. (22) observed two-monolayer-thick ZnO (0001) films grown on Ag substrates through surface X-ray diffraction and scanning tunneling microscopy, which provided a direct evidence for the presence of planar ZnO sheets. Recently, Lin et al. (24) prepared perpendicularly oriented ZnO nanosheets with a thickness of about 5 nm on a large scale, which showed feasible application in dye-sensitized solar cells. Through microwave thermal vapor technology, Wei et al. (25) successfully synthesized 2D single-crystal ZnO nanosheets with a thickness of 20−80 nm. Note that the high-quality ZnO thin sheets produced via most experimental routes, especially the pulsed laser deposition (PLD) technology (28), tend to prefer c-axis well-aligned orientation with a polar morphology.

The existence of polarized surfaces leads to an electrostatic instability resulting from the divergence of surface energy in the direction perpendicular to the polar surface. Several possible mechanisms have been proposed for stabilizing such polar features, including surface reconstruction (29), adsorption of H adatoms (30), transfer of electrons

between the (0001) and (000$\bar{1}$) surface (31), and surface termination by, for instance, hydrogen (32).

Very recently, first-principles computations have predicted that fully and partially hydrogenated graphene (33−37) and BN (38, 39) nanoribbons exhibit completely distinct properties from their pristine forms. In contrast, fundamental questions linked to wurtzite ZnO sheets remain unexplored. The surface Zn and O atoms are unsaturated compared with the bulk 4-fold coordination, and thus act as active sites for the adsorption of adatoms to form chemical bonds. The interaction of adatoms with polar ZnO surfaces has been extensively studied in connection with the unusual instability of polar surfaces. Theoretically, Wang et al. (40) and Chen et al. (41) predicted that surface fluorination provides an efficient route to induce intriguing electronic and magnetic properties of a few ZnO layers. Huang et al. (42) reported that surface passivations of H, F, Cl and NH$_2$ allow for the engineering of electronic states of wurtzite ZnO nanowires. Hydrogen is a common impurity during the preparation of ZnO materials; its frequent presence has once been considered responsible for the unintentional n-type semiconductivity of as-grown ZnO crystals (43). Hydrogen has also been demonstrated to lead to conductive and metallic ZnO (44). Several experimental efforts (45−47) have been devoted to hydrogen incorporation on the polar ZnO surfaces. Beker et al. (46) revealed the formation of a H (1 × 1) overlayer on the Zn-terminated ZnO(0001) surface through He-atom scattering technique. Quiet recently, the existence of surface hydrogen on the ZnO(000$\bar{1}$)−O surface has also been confirmed through X-ray photoelectron spectroscopy (47). Yet a theoretical understanding of electronic and magnetic properties of these functionalized ZnO nanosheets remains unclear.

Because the interaction of hydrogen with ZnO is of great technological interest, what properties distinguishable from unsaturated bare sheets will be present in a hydrogenated ZnO nanosheet? In addition, unlike graphene, whose carbon atoms are all chemically equivalent, the surface Zn and O atoms in ZnO sheet have different reacting and bonding natures with H atoms. How do the properties of a partially hydrogenated ZnO nanosheet depend on the saturated site? Among other important issues, how and to what extent does the sheet thickness affect the electronic and magnetic properties as well as the relative stabilities of different hydrogenated systems? The aim of the current study is to address the above questions. Density functional theory (DFT) computations were performed to systematically investigate the structural, electronic and magnetic properties of fully and partially hydrogenated ZnO nanosheets terminating with polar (0001)/(000$\bar{1}$) surfaces. These studies provide us a deep understanding of the novel properties of hydrogenated ZnO nanosheets, which is essential to employ them as building blocks for future nanodevices.

COMPUTATIONAL METHOD

DFT computations were performed using the plane-wave technique implemented in the Vienna ab initio simulation package (VASP). The ion-electron interaction is described with
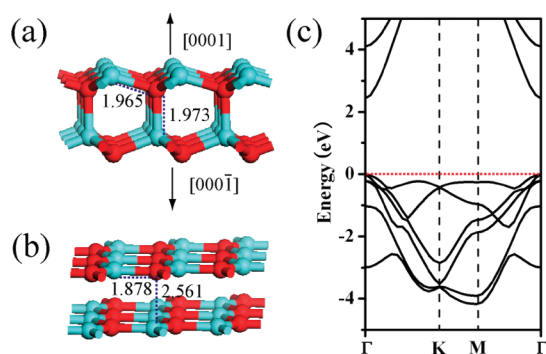

FIGURE 1. Structure of ZnO nanosheets with two bilayers: (a) initial wurtzite structure and (b) graphitic structure after optimization. The red and blue balls represent O and Zn atoms, respectively, and the numbers are bond length or interlayer distance in Å. (c) Band structure of b. The Fermi level is denoted with a red dashed line.

the projector augmented wave (PAW) method (48). The exchange-correlation potential is approximated by the generalized gradient approximation (GGA) using the PW91 functional (49) for both spin-polarized and spin-unpolarized cases. A 360 eV cutoff for the plane-wave basis set was used in all computations. All structures were treated with periodic boundary conditions, and the supercell was large enough to ensure a vacuum spacing greater than 10 Å. Pseudopotentials with $4s^2 3d^{10}$, $2s^2 2p^4$, and $1s^1$ valence electron configurations were used for Zn, O, and H atoms, respectively. The Brillouin zone was sampled by 4 × 4 × 4 and 5 × 5 × 1 special k points for ZnO bulk and 2D nanosheets, respectively. Geometry optimizations were performed by using the conjugated gradient method, and the convergence threshold was set to be 1 × 10^{-4} eV in energy and 1 × 10^{-3} eV/Å in force.

The ZnO nanosheets under investigation were constructed from the bulk phase, with the thickness ranging from one to five bilayers (a bilayer is composed of two closely adjacent layers, one for Zn and the other for O, e.g., the ZnO nanosheet in Figure 1a contains two bilayers).

RESULTS AND DISCUSSION

Bare ZnO Nanosheets. We began our study with ZnO wurtzite structure, in which all atoms are in sp^3 hybridization with each Zn (O) atom surrounded by four neighboring O (Zn) atoms at the corners of a tetrahedron. The Zn−O bond lengths within one bilayer and those between two adjacent bilayers are calculated to be 1.965 and 1.973 Å, respectively. The equilibrium cohesive energy per Zn−O pair, defined as the difference between the total energy of the optimized crystal structure and the corresponding isolated Zn or O atom, is calculated to be 7.532 eV, in good agreement with the experimental value (7.52 eV) (50). However, the band gaps of transition metal oxides are underestimated under GGA within DFT. We thus adopted the GGA + U method (51) to reassess the band structure of ZnO wurtzite crystal; this yielded a band gap of 1.77 eV. Although this is still much lower than the experimental value (∼3.4 eV), the GGA + U approach constitutes a significant improvement over the uncorrected GGA value (1.05 eV). Therefore, the GGA + U scheme was employed in all the following computations and analyses.

Next we studied 2D nanosheets derived from wurtzite ZnO. According to our computations, nanosheets composed of one to five bilayers transform from the initial wurtzite
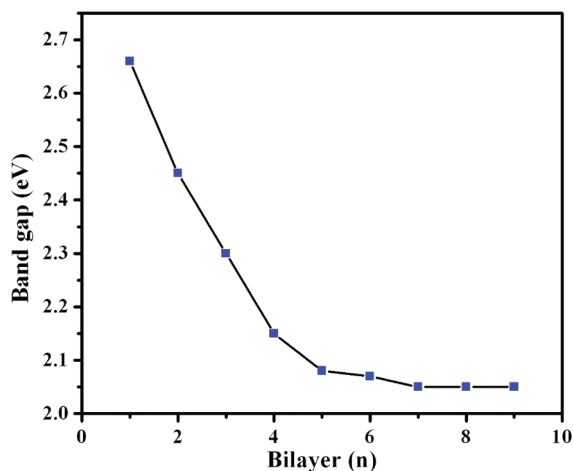
ACS **APPLIED** MATERIALS &INTERFACES

FIGURE 2. Band gap evolution of graphitic nanosheets as a function of bilayer number, n ($1 \leq n \leq 9$). n represents the number of bilayers in the initial wurtzite configuration, which forms a graphitic structure after geometry optimization.
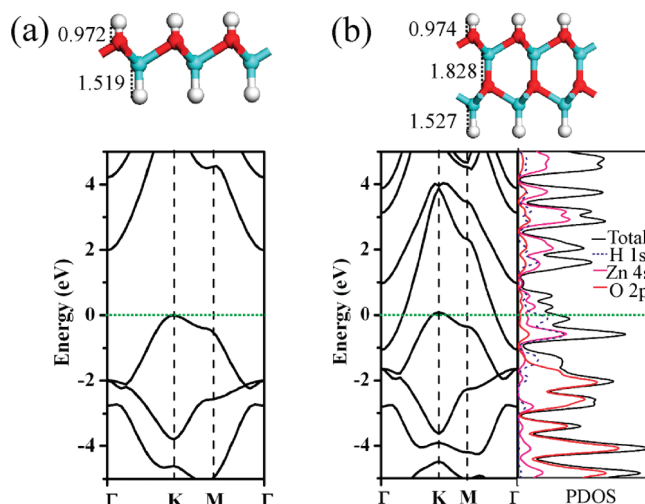

FIGURE 3. Optimized geometry and band structure for fully hydrogenated (a) one-bilayer (1-ZnO-2H) and (b) two-bilayer (2-ZnO-2H) sheets. Red, blue and white balls represent O, Zn, and H atoms, respectively. In b, PDOS is also shown for selected atomic orbitals.

configuration to a flat graphitic structure after geometry optimization, as exemplified by the two-bilayer-thick ZnO nanosheet in Figure 1. A pronounced geometry change appears in this case: the atoms within each bilayer converge to just one planar layer, accompanied by the Zn–O bond contraction (1.965–1.878 Å) within each bilayer and the interlayer distance expansion (1.973–2.561 Å). Moreover, the bond angle within the newly formed planar layer increases from the wurtzite tetrahedral, 109° on average, to plane trigonal, ~120°. Similar to the single-layer hexagonal ZnO, the two-layer graphitic ZnO is also a semiconductor with a direct band gap of 2.45 eV (Figure 1b).

Previous theoretical studies on the ultrathin films terminating with polar (0001)/(000$\bar{1}$) surfaces suggested that the energetically preferable graphitic structure occurs for only a limited number of layers. Specifically, for a ZnO wurtzite film, the graphitic-like conformation could persist only up to nine bilayers (52). To verify this prediction, we conducted a further study by examining ZnO wurtzite sheets with 6, 7, 8, 9, 10, and 11 bilayers. Our results confirm that the graphitic structure persists until nine bilayers and that thicker sheets (10 or 11 bilayers) recover the polar wurtzite (0001)/(000$\bar{1}$) configuration. Our results are in agreement with the previous report by Freeman et al. (52) at the same GGA level.

All the graphitic ZnO nanosheets considered here are semiconductors, and Figure 2 shows the evolution of band gap as a function of sheet thickness. Initially, the band gap monotonically decreases with increasing bilayer number, and then it converges to a thickness-independent constant of 2.05 eV. The larger band gaps for the thinner sheets are an indication of quantum size effect.

Fully Hydrogenated Wurtzite ZnO Nanosheets.

Following the idea of hydrogenated graphene (33) and h-BN (39) sheets, we then studied fully hydrogenated ZnO nanosheets with different thicknesses (denoted as n-ZnO-2H, where n refers to the number of bilayers). Figure 3 presents the relaxed geometry, band structure, and density of states (DOS) of fully hydrogenated one-bilayer (1-ZnO-2H, Figure 3a) and two-bilayer (2-ZnO-2H, Figure 3b) sheets, respec-

tively. The Zn and O atoms are in sp^3 hybridization with H atoms bonded to Zn and O atoms in the polar surface. Furthermore, the optimized Zn–H bond lengths (1.519 and 1.527 Å, respectively, for the hydrogenated one-bilayer and two-bilayer sheets) and O–H bond lengths (0.972 and 0.974 Å) indicate the formation of strong chemical bonds between hydrogen and surface atoms. The bond angles $\angle_{HOZn-1}$ ($\angle_{HOZn-2}$), $\angle_{HZnO-1}$ ($\angle_{HZnO-2}$), $\angle_{ZnOZn-1}$ ($\angle_{ZnOZn-2}$), and $\angle_{OZnO-1}$ ($\angle_{OZnO-2}$) corresponding to 1-ZnO-2H (2-ZnO-2H) are 120.7° (120.5°), 120.7° (120.8°), 96.3° (96.5°), and 96.3° (96.2°) on average, respectively. The optimized structural parameters suggest that the fully hydrogenated sheet retains the initial wurtzite configuration rather than the graphitic one.

Similar to graphene or monolayer BN sheets, the fully hydrogenated one-bilayer sheet (1-ZnO-2H) is a nonmagnetic semiconductor, with an indirect band gap of 2.07 eV, narrower than that of a bare ZnO graphitic sheet (2.66 eV, Figure 2). Interestingly, the hydrogenated sheets with thicknesses greater than one bilayer are all metallic. As exemplified in Figure 3b, the hydrogenated two-bilayer sheet (2-ZnO-2H) becomes a nonmagnetic metal (for 3, 4, and 5 bilayers, see Figure S1 in Supporting Information).

In ZnO nanostructures (53, 54), typically the absorbed H acts as an n-doping source, which donates electrons to occupy the 2p states of surface O atoms and 4s states of surface Zn atoms. The hybridized bonding state is located at the valence band maximum (VBM) and partially occupied, leading to the metallic behavior. This scenario also holds true for the fully hydrogenated ZnO sheets, as consolidated by the projected DOS (PDOS) in Figure 3b. The state crossing the Fermi level is mostly composed of the Zn 4s and O 2p state. The significant difference in electronic properties between one-bilayer and multibilayer sheet is closely related to their intrinsic surface states, which are completely removed after surface H passivation for the 1-ZnO-2H sheet, but only partially removed for the n-ZnO-2H ($n > 1$).
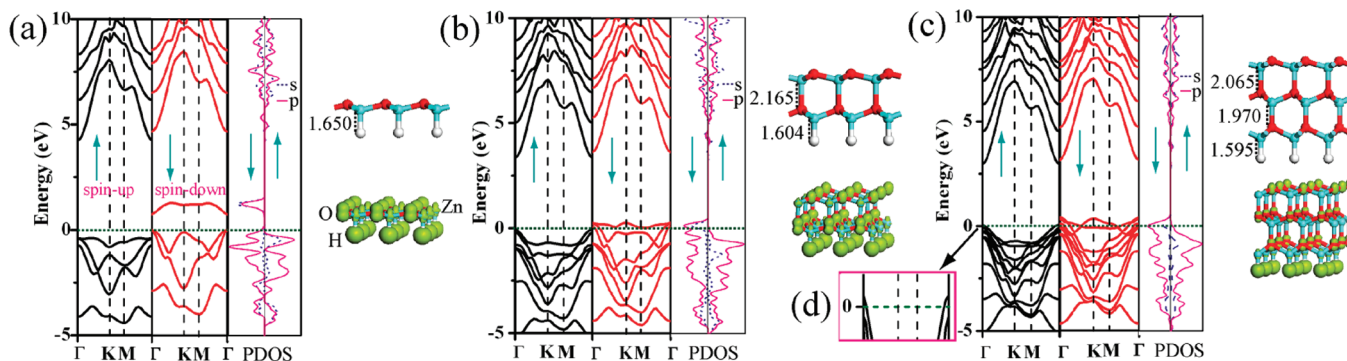
FIGURE 4. Optimized geometric structure (side view), band structure, PDOS, and spin density distribution of (a) 1-ZnO-ZnH, (b) 2-ZnO-ZnH, and (c) 3-ZnO-ZnH, respectively. (d) Zoom of the region near the Fermi level for the spin-up band structure of c. The isosurface is set to be 0.05 e/Å^3.

Bare ZnO nanosheets of fewer than 9 bilayers favor a flat graphitic structure after relaxation and are semiconductors. In contrast, all fully hydrogenated ZnO nanosheets, except the one-bilayer sheet, adopt the wurtzite configuration and are metallic. This conspicuous difference indicates that the structural and electronic properties of ZnO nanosheets are very sensitive to surface decoration.

Semihydrogenation on Zn Sites for ZnO Nanosheets. Similar to B and N sites in BN sheets, Zn and O sites in ZnO nanosheets are chemically nonequivalent, and then semihydrogenation can be achieved by merely saturating either all the Zn sites or all the O sites. We first studied semihydrogenation on Zn sites for ZnO nanosheets with different numbers of bilayers (denoted as n-ZnO-ZnH).

In Figure 4 we summarize the results of semihydrogenated ZnO sheets with one, two and three bilayers (for four and five bilayers, see Figure S2 in Supporting Information). In all cases, spin polarization is evident in the band structure and PDOS. In fact, semihydrogenation on Zn atoms forms strong Zn−H bonds and leaves the dangling bonds of surface O atoms spin unpaired. The origin of the magnetic behavior was further investigated by plotting the spin density distribution (Figure 4). Obviously, the emergent spin polarization is not restricted to the surface O atoms but instead is delocalized uniformly in the entire system, leading to a net magnetic moment of approximately 0.67, 0.66, 0.39, 0.31, and 0.27 μ_B per unit cell for one, two, three, four, and five bilayers, respectively. The induced magnetism is attributed primarily to unsaturated O atoms (2p$_z$ orbital) and H atoms (1s orbital), with a little contribution from Zn atoms (3d orbital).

More careful examination of the band structure of n-ZnO-ZnH reveals appealing properties associated with this novel system. As described in Figure 4a, the hydrogenated one-bilayer system (1-ZnO-ZnH) behaves as a magnetic semiconductor with direct band gaps of 4.69 and 0.75 eV in the spin-up and spin-down state, respectively. The absorption of H atom on Zn sites introduces a low acceptor level located slightly above the VBM, which is spin-polarized with only one spin channel completely occupied, resulting in hole-doping p-type semiconductivity. However, when the thickness increases to two bilayers, the resulting 2-ZnO-ZnH becomes a magnetic half-metal. As clearly seen in Figure 4b, the spin-up state behaves as a semiconductor with a direct band gap of 3.39 eV, whereas the spin-down state turns metallic.
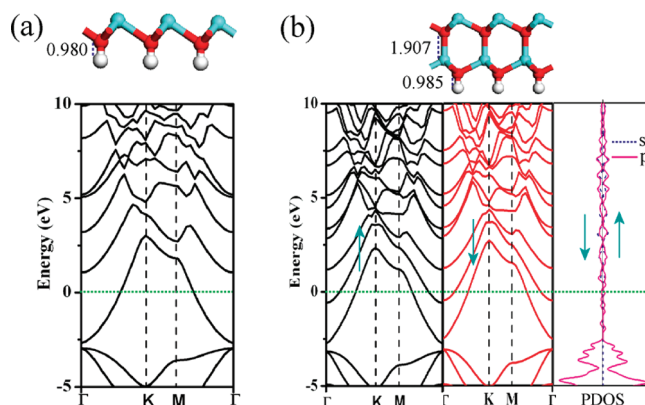

FIGURE 5. Optimized geometry (side view) and band structure for (a) 1-ZnO-OH and (b) 2-ZnO-OH with PDOS.

Interestingly, when the number of bilayers further increases to three, both the spin-up and spin-down states become metallic, as can be seen in c and d in Figure 4. The situation for four and five bilayers is similar to that of three (see Figure S2 in Supporting Information), indicating that the semihydrogenated multilayer sheets are all metals with strong spin polarization.

This remarkable phenomenon can be further scrutinized by analyzing the nature of the Zn−H bonds (Figure 4). Noticeably, the Zn−H bond length decreases drastically as the thickness increases, indicating the reinforcement of Zn−H bonds. This bond strengthening is accompanied by a reduction of interlayer distance, which stabilizes the structure. The hydrogen-derived bands are significantly affected by the bonding variation. By increasing the thickness, both occupied spin-up and unoccupied spin-down channels are broadened because of the hybridization effect, which makes the Fermi level lie in the H-induced bands and gives rise to half-metallic or metallic behaviors. Thus, with semihydrogenation restricted on the surface Zn atoms, a magnetic p-type semiconductor → half-metal → metal transition can be tuned by varying the sheet thickness.

Semihydrogenation on O Sites for ZnO Nanosheets. Figure 5 presents the results of semihydrogenation on O sites (denoted as n-ZnO-OH), in one- and two-bilayer sheets (for three, four, and five bilayers, see Figure S3 in Supporting Information). In contrast with 1-ZnO-ZnH, 1-ZnO-OH is practically a nonmagnetic metal (Figure 5a). Nevertheless, spin-polarized states appear for thicker sheets (two, three,

FIGURE 6. Summary of the electronic and magnetic properties of (a) *n*-ZnO-2H, (b) *n*-ZnO-ZnH, and (c) *n*-ZnO-OH with different numbers of bilayers.

four, and five bilayers). The spin-polarized magnetization mainly comes from the 2p orbital of the O atom. The calculated magnetic moments are 0.11, 0.06, 0.03, and 0.02 μ_B per unit cell for sheets with two, three, four, and five bilayers, respectively. Thus, semihydrogenation on Zn sites possesses an essentially larger magnetic moment than that on O sites. This is easily understandable that the dangling bonds on Zn atoms (as in ZnO-OH) exhibit much less spin density compared with those of unpaired O atoms (as in ZnO-ZnH). Moreover, unlike *n*-ZnO-ZnH, the optimized O–H bond lengths in *n*-ZnO-OH tend to increase with thickness, suggesting the weakening of bonds between O and H atoms.

Furthermore, all semihydrogenated systems on O sites are strikingly metallic irrespective of thickness. This is consistent with Jia et al.'s report (55) that [0001] ZnO nanowires with only O atoms saturated by atomic H on the side surface are metallic. As mentioned above, the induced metallicity is attributed to the partially occupied surface state, which is not completely removed after hydrogen passivation.

Finally, we summarize the computed properties for hydrogenated ZnO nanosheets in Figure 6. Clearly, the intriguing and diverse transformation in electronic and magnetic properties of the novel ZnO systems depends remarkably on hydrogenation sites and sheet thickness. Our results predict that effectively controlling the hydrogenation sites and sheet thickness is a tunable way to modulate the properties of ZnO nanosheets, and that a semiconductor → half-metal → metal (nonmagnetic-magnetic) transition can be achieved. We have additionally investigated ZnO sheet with 9 bilayers. The fully hydrogenated ZnO sheet with 9 bilayers remains a nonmagnetic metal as those with 2−5 bilayers. Partially hydrogenated ZnO sheets on surface Zn and O atoms are both magnetic metals (see Figure S4 in Supporting Information). Obviously, the ZnO nanosheets thicker than 5 bilayers follow the trend summarized in Figure 6. These diverse properties are of fundamental significance and open up exciting opportunities for the design of novel nanoelectronic spintronic devices.

Stabilities of Fully and Partially Hydrogenated ZnO Nanosheets. To evaluate the structural stability of the hydrogenated ZnO sheets, we calculated the formation energies for both fully and partially hydrogenated systems. The formation energy (E_f) is expressed as $E_f = E_{ZnO-H} - (\chi_{Zn-O}\mu_{Zn-O} + \chi_H\mu_H)$, where E_{ZnO-H} is the cohesive energy per atom of hydrogenated nanosheet, μ_{Zn-O} is the cohesive energy per
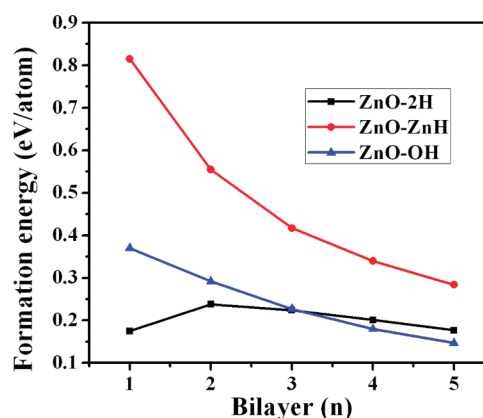

FIGURE 7. Formation energies of hydrogenated ZnO sheets as a function of bilayer number, *n*. ZnO-2H denotes the fully hydrogenated ZnO nanosheet, and ZnO-ZnH and ZnO-OH are the nanosheets semihydrogenated at Zn and on O sites, respectively.

Zn–O pair of bulk wurtzite ZnO, μ_H is half of the binding energy of H_2, and χ_{Zn-O} (χ_H) is the molar fraction of Zn–O pairs (H atom) in the hydrogenated systems. According to this definition, a system with smaller E_f value is more favorable.

Figure 7 shows the relative stability of different ZnO systems as a function of bilayer number. For the semihydrogenated case (*n*-ZnO-ZnH or *n*-ZnO-OH), the comparison of relative stability is straightforward: the formation energy progressively decreases with increasing bilayer number, which suggests that thicker sheets are more likely to be accessible; moreover, with the same bilayer number, *n*-ZnO-OH is energetically more preferable than *n*-ZnO-ZnH. However, the fully hydrogenated systems are more complicated. When the thickness is fewer than three bilayers, the fully hydrogenated system (*n*-ZnO-2H) is more favorable than its semihydrogenated counterpart, but for thicker sheets the most stable system is *n*-ZnO-OH. For all the ZnO nanosheets considered, semihydrogenated ones at Zn sites are the least stable.

CONCLUSION

In summary, we have systematically investigated the structural, electronic and magnetic properties of ZnO nanosheets. Bare wurtzite ZnO nanosheets with fewer than nine bilayers adopt a graphite-like structure after atomic relaxation. Hydrogen saturation of surface atoms can transform these ZnO nanosheets into wurtzite configurations. The fully hydrogenated ZnO sheet with a single bilayer is an indirect band gap

semiconductor, whereas those with thicker bilayers become metallic independent of thickness. The semihydrogenated sheets on Zn sites are all magnetic, and a semiconductor → half-metal → metal transition occurs with increasing sheet thickness. Semihydrogenation on O sites results in nonmagnetic metallicity in a ZnO monolayer sheet and weakly magnetic metallicity in multilayer sheets. Furthermore, the fully hydrogenated ZnO nanosheets containing fewer than three bilayers are energetically more favorable than their semihydrogenated counterparts. For thicker sheets, ZnO nanosheets semihydrogenated at O sites are more favorable energetically. Thus, surface passivation by hydrogen serves as an important approach in tailoring the electronic and magnetic properties of low-dimensional ZnO nanosheets.

Our computations revealed that the polar surfaces of wurtzite sheets are highly active and easily susceptible to atomic adsorption. We are quite confident that our experimental peers will realize the appealing electronic and magnetic properties associated with the ZnO nanosheets studied in this work. In addition to the hydrogen decoration, surface saturation by other functional groups or chemical/physical modification of ZnO nanosheets may further tune these electronic and magnetic properties. The properties predicted here for ZnO nanosheets may also be extended to other wurtzite nanostructures such as GaN and CdS.

Supporting Information Available: Geometry and band structures of fully and partially hydrogenated ZnO nanosheets with three, four, five, and nine bilayers (PDF). This material is available free of charge via the Internet at http://pubs.acs.org.

REFERENCES AND NOTES

(1) Özgür, Ü.; Alivov, Y. I.; Liu, C.; Teke, A.; Reshchikov, M. A.; Doğan, S.; Avrutin, V.; Cho, S. J.; Morkoc, H. *J. Appl. Phys.* **2005**, *98*, 041301.
(2) Tsukazaki, A.; Ohtomo, A.; Onuma, T.; Ohtani, M.; Makino, T.; Sumiya, M.; Ohtani, K.; Chichibu, S. F.; Fuke, S.; Segawa, Y.; Ohno, H.; Koinuma, H.; Kawasaki, M. *Nat. Mater.* **2004**, *4*, 42.
(3) Law, M.; Greene, L. E.; Johnson, J. C.; Saykally, R.; Yang, P. D. *Nat. Mater.* **2005**, *4*, 455.
(4) Maeda, K.; Takata, T.; Hara, M.; Saito, N.; Inoue, Y.; Kobayashi, H.; Domen, K. *J. Am. Chem. Soc.* **2005**, *127*, 8286.
(5) Irimpan, L.; Nampoori, V. P. N.; Radhakrishnan, P. *Sci. Adv. Mater.* **2010**, *2*, 117.
(6) Wang, H.; Huang, H.; Wang, B. *Sci. Adv. Mater.* **2010**, *2*, 184.
(7) Seif, A.; Boshra, A. *J. Comput. Theor. Nanosci.* **2009**, *6*, 732.
(8) Wang, Z. L. *J. Phys.: Condens. Matter* **2004**, *16*, R829.
(9) Wang, X. D.; Song, J. H.; Li, P.; Ryou, J. H.; Dupuis, R. D.; Summers, C. J.; Wang, Z. L. *J. Am. Chem. Soc.* **2005**, *127*, 7920.
(10) Zhang, B. P.; Binh, N. T.; Wakatsuki, K.; Segawa, Y. *Appl. Phys. Lett.* **2004**, *84*, 4098.
(11) Pan, Z. W.; Dai, Z. R.; Wang, Z. L. *Science* **2001**, *291*, 1947.
(12) Yin, M.; Gu, Y.; Kuskovsky, I. L.; Andelman, T.; Zhu, Y.; Neumark, G. F.; O'Brien, S. *J. Am. Chem. Soc.* **2004**, *126*, 6206.
(13) Lao, J. Y.; Huang, J. Y.; Wang, D. Z.; Ren, Z. F. *Nano Lett.* **2003**, *3*, 235.
(14) Govender, K.; Boyle, D. S.; Kenway, P. B.; O'Brien, P. *J. Mater. Chem.* **2004**, *14*, 2575.
(15) Kong, X. Y.; Ding, Y.; Yang, R.; Wang, Z. L. *Science* **2004**, *303*, 1348.
(16) Topsakal, M.; Cahangirov, S.; Bekaroglu, E.; Ciraci, S. *Phys. Rev. B* **2009**, *80*, 235119.
(17) Kulkarni, A. J.; Min, Z.; Sarasamak, K.; Limpijumnong, S. *Phys. Rev. Lett.* **2006**, *97*, 105502.
(18) Botello-Méndez, A. R.; López-Urías, F.; Terrones, M.; Terrones, H. *Nano Lett.* **2008**, *8*, 1562.
(19) Kou, L.; Li, C.; Zhang, Z.; Guo, W. *ACS Nano* **2010**, *4*, 2124.
(20) Kou, L.; Li, C.; Zhang, Z.; Guo, W. *J. Phys. Chem. C* **2010**, *114*, 1326.
(21) Chen, Q.; Zhu, L.; Wang, J. *Appl. Phys. Lett.* **2009**, *95*, 133116.
(22) Tusche, C.; Meyerheim, H. L.; Kirschner, J. *Phys. Rev. Lett.* **2007**, *99*, 026102.
(23) Gao, P.; Chen, Y.; Wang, Y.; Zhang, Q.; Li, X.; Hu, M. *Chem Commun* **2009**, 2762.
(24) Lin, H.; Lin, C.; Zhuang, D.; Li, X.; Li, J. *Int. J. Mater. Prod. Technol.* **2010**, *37*, 305.
(25) Wei, G.; Qin, W.; Ning, L.; Kim, R.; Wang, G.; Zhang, D.; Zhu, P.; Zheng, K.; Wang, L. *J. Nanosci. Nanotechnol.* **2010**, *10*, 2065.
(26) Wang, N.; Lin, H.; Li, J.; Zhang, L.; Li, X.; Wu, J.; Lin, C. *J. Am. Chem. Soc.* **2007**, *90*, 635.
(27) Chen, S.; Liu, Y.; Shao, C.; Mu, R.; Lu, Y.; Zhang, J.; Shen, D.; Fan, X. *Adv. Mater.* **2005**, *17*, 586.
(28) Sun, X. W. *J. Appl. Phys.* **1999**, *86*, 408.
(29) Dulub, O.; Boatner, L. A.; Diebold, U. *Surf. Sci.* **2002**, *519*, 201.
(30) Fritsch, J.; Sankey, O. F.; Schmidt, K. E.; Page, J. B. *Phys. Rev. B* **1998**, *57*, 15360.
(31) Wander, A.; Schedin, F.; Steadman, P.; Norris, A.; McGrath, R.; Turner, T. S.; Thornton, G.; Harrison, N. M. *Phys. Rev. Lett.* **2001**, *86*, 3811.
(32) Wander, A.; Harrison, N. M. *J. Chem. Phys.* **2001**, *115*, 2312.
(33) Sofo, J. O.; Chaudhari, A. S.; Barber, G. D. *Phys. Rev. B* **2007**, *75*, 153401.
(34) Elias, D. C.; Nair, R. R.; Mohiuddin, T. M. G.; Morozov, S. V.; Blake, P.; Halsall, M. P.; Ferrari, A. C.; Boukhvalov, D. W.; Katsnelson, M. I.; Geim, A. K.; Novoselov, K. S. *Science* **2009**, *323*, 610.
(35) Li, Y.; Zhou, Z.; Shen, P.; Chen, Z. *J. Phys. Chem. C* **2009**, *113*, 15043.
(36) Barone, V.; Hod, O.; Scuseria, G. E. *Nano Lett.* **2006**, *6*, 2748.
(37) Zhou, J.; Wang, Q.; Sun, Q.; Chen, X. S.; Kawazoe, Y.; Jena, P. *Nano Lett.* **2009**, *9*, 3867.
(38) Zhou, J.; Wang, Q.; Sun, Q.; Jena, P. *Phys. Rev. B* **2010**, *81*, 085442.
(39) Chen, W.; Li, Y.; Yu, G.; Li, C.; Zhang, S. B.; Zhou, Z.; Chen, Z. *J. Am. Chem. Soc.* **2010**, *132*, 1699.
(40) Wang, Y.; Ding, Y.; Ni, J.; Shi, S.; Li, C.; Shi, J. *Appl. Phys. Lett.* **2010**, *96*, 213117.
(41) Chen, Q.; Wang, J.; Zhu, L.; Wang, S.; Ding, F. *J. Chem. Phys.* **2010**, *132*, 204703.
(42) Huang, S.; Xu, H.; Bello, I.; Zhang, R. Q. *J. Phys. Chem. C* **2010**, *114*, 8861.
(43) Shi, G. A.; Saboktakin, M.; Stavola, M. *Appl. Phys. Lett.* **2004**, *85*, 5601.
(44) Wang, Y.; Meyer, B.; Yin, X.; Kunat, M.; Langenberg, D.; Traeger, F.; Birkner, A.; Woll, C. *Phys. Rev. Lett.* **2005**, *95*, 266104.
(45) Bruno, G.; Giangregorio, M. M.; Malandrino, G.; Capezzuto, P.; Fragalà, I. L.; Losurdo, M. *Adv. Mater.* **2009**, *21*, 1700.
(46) Becker, Th.; Hövel, St.; Kunat, M.; Boas, Ch.; Burghaus, U.; Wöll, Ch. *Surf. Sci.* **2001**, *486*, L502.
(47) Doh, W. H.; Roy, P. C.; Kim, C. M. *Langmuir* **2010**; DOI: 10.1021/la101369r.
(48) Blöchl, P. E. *Phys. Rev. B* **1994**, *50*, 17953.
(49) Perdew, J. P.; Chevary, J. A.; Vosko, S. H.; Jackson, K. A.; Pederson, M. R.; Singh, D. J.; Fiolhais, C. *Phys. Rev. B* **1992**, *46*, 6671.
(50) Weast, R. C.; Astle, M. J.; Beyer, W. H. *CRC Handbook of Chemistry and Physics*; CRC Press: Boca Raton, FL, 1986.
(51) Erhart, P.; Albe, K.; Klein, A. *Phys. Rev. B* **2006**, *73*, 205203.
(52) Freeman, C. L.; Claeyssens, F.; Allan, N. L. *Phys. Rev. Lett.* **2006**, *96*, 066102.
(53) Hofmann, D. M.; Hofstaetter, A.; Leiter, F.; Zhou, H.; Henecker, F.; Meyer, B. K. *Phys. Rev. Lett.* **2002**, *88*, 045504.
(54) McCluskey, M. D.; Jokela, S. J.; Zhuravlev, K. K.; Simpson, P. J.; Lynn, K. G. *Appl. Phys. Lett.* **2002**, *81*, 3807.
(55) Jia, J.; Shi, D.; Zhao, J.; Wang, B. *Nanotechnology* **2007**, *18*, 455708.

AM100467J